Applied Catalysis B: Environmental 209 (2017) 669–678

Contents lists available at ScienceDirect

Applied Catalysis B: Environmental

journal homepage: www.elsevier.com/locate/apcatb

An efficient selective reduction of nitroarenes catalyzed by reusable silver-adsorbed waste nanocomposite

Somnath Giri [a], Raghunath Das [a], Chris van der Westhuyzen [b], Arjun Maity [a,c,*]

[a] Department of Chemical Engineering, University of South Africa, Muckleneuk 0003, South Africa
[b] CSIR Biosciences, Pretoria, South Africa
[c] National Centre for Nanostructured Materials, Materials Science and Manufacturing, Council for Scientific and Industrial Research (CSIR), Pretoria, South Africa

ARTICLE INFO

Article history:
Received 29 November 2016
Received in revised form 1 March 2017
Accepted 9 March 2017
Available online 19 March 2017

Keywords:
Remediation
Waste
Ag nanoparticles
Nitroarene reduction
Reusable

ABSTRACT

Silver nanocomposites (AgNCs) were produced by adsorption onto an electron-rich polypyrrole-mercaptoacetic acid (PPy-MAA) composite, known to be a highly efficient adsorbent for the removal of Ag^+ ions from aqueous media in the remediation of metal- contaminated water sources. In situ reduction of Ag^+ cations to Ag^0 nanoparticles (NPs) was achieved in the absence of an additional reducing agent, and the AgNCs formed were characterized by FE-SEM, EDAX, HR-TEM, STEM, XRD, ATR-FTIR, and XPS. An investigation into the potential application of these AgNCs, effectively a waste product for further processing, as a catalyst for the reduction of variously substituted nitroarenes in water was undertaken in an effort to beneficiate the materials and determine the reaction's specificity. One composite having 11.14 ± 0.05 wt% Ag content was particularly active in these reductions, with aniline derivatives being prepared in 71–94% yields. The kinetics of the reaction was examined using 4- nitrophenol, a common water-soluble pollutant; pseudo-first-order kinetics was observed with predicted activation energy of 68.3 kJ/mol for this system. Furthermore, this AgNC displayed superior stability over 10 reaction cycles without loss of catalytic activity. A mechanism was elucidated based on these findings. The mild, economical, and efficient reduction method using a reusable "waste" material may prove a promising alternative for further industrial application.

1. Introduction

In recent years, the use of heterogeneous catalysts to promote the efficiency and the sustainability of reactions in organic synthesis has aroused considerable attention [1–3]. Additionally, principles such as waste minimization, the use of metal-incorporated waste material as catalysts, performing reactions open to the atmosphere at ambient temperature and pressure are key considerations [4–6]. In particular, the use of a retrievable catalyst from a reaction using water as solvent is highly attractive from an environmental standpoint [7]. From the point of view of the catalyst, the use of solid supports [8–13], such as activated carbon [8,9], polymers [10], alumina [11], zeolites [12], and TiO_2 [13] have conferred increased stability, reactivity, selectivity, and reusability of specifically metal nanoparticles. Such metal nanomaterials [14–16] and other bimetallic nanocatalysts [17–20] have been widely employed in various catalytic protocols.

Substituted aromatic amines are versatile important building blocks in preparation of fine chemicals, pigments, dyes, agrochemicals, pharmaceuticals, and biotechnology [21,22]. In addition, they form the basis of many common chemical intermediates such as amides, azo compounds, diazonium salts, and imines [23]. Aromatic amines are commonly prepared by catalytic reduction of nitroarenes using noble metal complexes and metal nanoparticles derived from Rh [24,25], Ru [26], Pt [27,28], Pd [29,30], Au [31], Ag [32], Ir [33] and Ni [34] among others. These are usually used in combination with hydrazine, CO/H_2O, alcohols, ammonium formate, hydrosilanes, and sodium borohydride or ammonia borane as hydrogen sources. Additionally, stoichiometric reducing agents [35–37] derived from iron, zinc, tin and copper have been used, particularly the Fe/HCl system. Another typical method uses Raney nickel as catalyst; its pyrophoric nature, operationally com-

* Corresponding author at: National Centre for Nanostructured Materials, Materials Science and Manufacturing, Council for Scientific and Industrial Research (CSIR), Pretoria, South Africa.
E-mail addresses: maityarjun@gmail.com, amaity@csir.co.za (A. Maity).

http://dx.doi.org/10.1016/j.apcatb.2017.03.033
0926-3373/

plex handling, and moisture sensitivity detract from its utility [38]. However, iron-catalyzed reduction systems are considered a viable alternative, due to the abundance, cost-effectiveness and lower toxicity of these catalysts. Several iron-catalyzed nitroarene reductions have been established under various conditions [39–41]. In general, however, serious environmental concerns have been raised over the use of most of these metal catalyst systems, particularly the use of acid, stoichiometric loading of reagents, lower selectivity, harsh reaction conditions, and expense associated with these materials. Another challenge associated with the reduction of nitroarenes is selectivity and compatibility with other functionality in the system. In this respect, gold catalysts have proved efficient at reducing nitro derivatives to anilines with excellent selectivitywith the associated expense [42,43] . Several methods by Beller and co-workers for the selective hydrogenation using iron catalysts with different molecular hydrogen, hydrazine hydrate, and formic acid have also been developed [44,45]. Quantitative conversion and high selectivity in these cases are offset by the need for specialized phosphine- or nitrogen-containing ligands, the use of organic solvents, and prolonged reaction time. Ranu and co-workers employed iron nanoparticles to chemoselectively reduce nitro derivatives using water as hydrogen source [46]. Recently, Bhanage et al. reported the use of a recyclable immobilized iron-based ionic liquid and hydrazine hydrate to chemoselectively and regioselectively reduce nitroarenes, albeit under reflux over a prolonged reaction time [47]. Interestingly, a readily available organocatalyst, vasicine, has been shown to chemoselectively reduce nitroarenes under metal-free and base-free conditions in water [48].

Synthetic concerns aside, from an environmental perspective, 4- nitrophenol (4-NP) is one of the most common toxic and biologically stable organic pollutants in industrial and agricultural wastewater derived from the preparation and use of dyes, pesticides and pharmaceuticals [49]. Simple reduction to 4-aminophenol (4-AP) reduces this toxicity, the product being an important structural intermediate in analgesic and antipyretic drugs, such as paracetamol and phentacin [50]. A number of catalytic reduction methods have been developed to reduce nitroarenes in order to remediate polluted wastewater streams. These include photocatalytic degradation, electrochemical methods, the electro-Fenton process, and catalytic oxidation processes [51,52]. Furthermore, several metal nanoparticles have been explored as a means to convert 4-NP to 4-AP using $NaBH_4$ as a generally acceptable reductant [53–55], with Pradhan and co- workers being first in reporting the use of silver nanoparticles for this purpose [56]. Hence, there is still scope for an efficient, mild and cost-effective method for nitroarene reduction in both the chemical and environmental areas utilizing sustainable heterogeneous catalysis. In this context, the catalytic hydrogenation of nitroarenes to their corresponding anilines has been investigated using reusable silver-adsorbed waste nanocomposites under mild reaction conditions.

In this present work, an efficient polymeric composite, the polypyrrole-mercaptoacetic acid incorporated polymer matrix (PPy-MAA), is reported as an excellent adsorbent for removing silver ions from aqueous streams – from the point of view of water remediation. The formation of well-structured silver nanoparticles in the matrix is demonstrated and characterized by ATR-FTIR, FE-SEM, HR-TEM, XRD and XPS techniques. In continuation of our ongoing research into the application of metal nanoparticles in catalysis [57], the silver-impregnated polymeric materials produced, effectively waste products requiring disposal, were beneficiated by applying the materials produced to the catalytic reduction of a variety of nitroarenes including 4-NP under mild reaction conditions. Catalyst performance from a kinetic, mechanistic and recyclability point of view is also considered.

2. Experimental

2.1. Chemicals

Pyrrole (Py, 99%), thioglycolic acid (mercaptoacetic acid) (≥98%), all nitro compounds, sodium borohydride ($NaBH_4$) and ammonium persulfate (APS) were purchased from Sigma-Aldrich, USA. Silver nitrate ($AgNO_3$, ≥99.0%) and acetone (ACS reagent, ≥99.5%) were supplied from Sigma-Aldrich, USA and were used as received. All the reactions were carried out in ultrapure distilled water (collected from an EASY pure®II, UV-ultrapure water system) open to atmosphere.

2.2. Preparation of PPy-MMA composite

The PPy/MAA composite was synthesized by dissolving 1.6 mL (23 mmol) mercaptoacetic acid in 60 mL of ultrapure water in a 250 mL conical flask with constant stirring at 400 rpm. Pyrrole (Py) (0.8 mL, 11.4 mmol) was added to this solution by syringe in one portion, and the homogeneous reaction was stirred for 30 min. 20 mL of ammonium persulfate (APS, 6.8 g ~30 mmol) was added dropwise to the solution and stirred for a further 6 h. Polymerization of Py was evident by the gradual development of a black composite material. The composite was filtered off and washed repeatedly with ultrapure water followed by acetone, and then dried under vacuum at 60 °C for 6 h to a constant weight. A plausible explanation for polymerization of Py monomer is based on the well- established oxidative mechanism indicating that ammonium persulphate (APS) generates free radical sites on the pyrrole backbone. These free radical sites react with another monomer and then propagate. After termination, polymer was precipitated in the ploymerization reaction medium. During polymerization, the growing PPy chain carries a positive charge on the nitrogen atoms in the reaction medium as a result of acid-base reactions with the MAA [58] . The mercaptoacetate moieties are expected to remain associated with the polypyrrole networks through electrostatic interaction, as later characterization implied.

2.3. Adsorption of Ag(I) ions onto PPy-MAA composite to form PPy- MAA/Ag nanocomposite catalyst

The adsorption of silver ions (Ag^+) from aqueous solution was conducted in batch experiments using the PPy/MAA composite at room temperature (25 °C) while stirring at 200 rpm with an overhead stirrer. To evaluate the capacity of the PPy-MMA for Ag^+ adsorption, five different experimental solutions, i.e. 10, 25, 50, 100 and 200 mg/L were prepared from a stock solution (1000 mg/L) of $AgNO_3$. For each experimental solution, 0.4 g of PPy/MAA adsorbent was added to 1 L of Ag^+ solution at pH 5.4. After 24 h, the solution was filtered through 0.45 μm membrane filter paper and the filtrate was analyzed by ICP-MS (Thermo Fisher Scientific) to determine the residual concentration of metal ion (Ag^+) in the filtrate. The adsorption equilibrium capacity (q_e, mg/g) for Ag^+ adsorption on the PPy/MAA composite was calculated using Eq. (1).

$$q_e(\mathrm{mg/g}) = \frac{(C_0 - C_e)V}{W} \quad (1)$$

where q_e is the adsorption capacity (mg/g) at equilibrium; C_0 and C_e are the initial and the equilibrium concentrations (mg/L) of Ag^+ ions respectively; V is the volume of the experimental solution (L), and W is the weight of the adsorbent (g). The PPy-MAA/Ag^+ composite was collected for use in the reduction of 4-NP. Five different catalysts having different wt% of silver were collected these processes: Ag NC-1 (11.14 ± 0.05 wt%); Ag NC-2 (19.75 ± 0.05 wt%); Ag NC-3 (32.51 ± 0.05 wt%); Ag NC-4 (5.83 ± 0.05 wt%); Ag NC-5 (2.42 ± 0.05 wt%). From XRD, XPS, FE-SEM and HR-TEM studies, it

Table 1

Optimization of reaction conditions.[a]

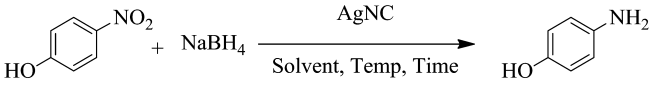

Entry	Catalyst	Catalyst (mol%)	$NaBH_4$ (equiv.)	Solvent	Time (h)	Selectivity (%)	Yield (%)[b]
1	AgNC-3[f]	5	10	H_2O	4.5	100	84
2	AgNC-2[f]	5	10	H_2O	3.5	100	88
3	AgNC-1[f]	5	10	H_2O	2	100	94
4	AgNC-1[f]	5	10	MeOH	5	100	51
5	AgNC-1[f]	5	10	EtOH	5	100	62
6	AgNC-1[f]	2.5	10	H_2O	6	100	82
7	AgNC-1[f]	1.5	10	H_2O	8	100	71
8	AgNC-1[f]	2.5	5	H_2O	9	100	67
9	AgNC-1[f]	5	5	H_2O	5	100	81
10	PPy-MAA	50 mg	10	H_2O	24	–	–[c]
11	No catalyst	none	10	H_2O	24	–	–[d]
12	AgNC-1[f]	5	none	H_2O	24	–	–[e]

[a] Reaction conditions: **1** (1 mmol), catalyst (5 mol %), solvent (10 mL), room temperature (25 °C).
[b] Isolated yields of **1a**.
[c] With PPy-MAA composite (50 mg).
[d] Without catalyst.
[e] Without $NaBH_4$.
[f] AgNC-1, -2, -3 with 11.14 ± 0.05, 19.75 ± 0.05, and 32.51 ± 0.05 wt% Ag, respectively.

was determined that the adsorbed Ag^+ ions existed as Ag^0 as a result of reduction by the electron-rich PPy-MAA polymeric matrix [59]. It was also found from Table 1 that Ag NC-1 provided better results than Ag NC-2 and Ag NC-3 for the catalytic reaction of 4-nitrophenol. Thereafter, Ag NC-1 was chosen for the rest of the studies. In this study, Ag NC-1 was fully characterized using ATR-FTIR, FE-SEM, HR-TEM, XRD and XPS.

2.4. General information of characterization techniques

The surface morphology and elemental composition of AgNC-1 were determined using Field Emission-Scanning Electron Microscope (FE-SEM) with an energy dispersive X- ray spectrometer (EDX) (Carl Zeiss, Germany). TEM and Scanning Transmission Electron Microscope (STEM) photographs of the catalyst were acquired using a JEOL JEM-2100 instrument with a LAB6 filament operating at 200 kV. FTIR spectral analysis was performed using a Perkin-Elmer Spectrum 100 ATR-FTIR spectrometer with scanning range of 600–4000 cm^{-1} at a resolution of 4 cm^{-1}/s. The powder X-ray iffraction (XRD) patterns of the catalyst before reaction and after 10th cycle of the catalytic reaction were studied using a PANalytical X'Pert PRO-diffractometer with a Cu Kα radiation source (wavelength, λ = 1.5406 Å), and angular variation of 5–90° operated at a generator voltage and current of 40 kV and 40 mA respectively. Oxidation states of the elements of the catalyst were obtained using high-resolution X-ray photoelectron spectroscopy (XPS) on a Kratos Axis Ultra device, with focused monochromatized Al Kα radiation source ($h\nu$ = 1486.6 eV). Catalytic reduction of 4-nitrophenol (4-NP) was studied using a UV-vis spectrophotometer (Perkin Elmer, Lambda 35). The wt% of the silver present in the catalyst and leaching test were determined using an inductively Coupled Plasma Mass Spectrometer (ICP-MS) (Thermo Fisher Scientific). Analytical thin layer chromatography (TLC) was performed using Kieselgel 60 F-254 on aluminium sheets and visualization was accomplished by using either UV light or I_2 vapor to stain the plates. Unless otherwise noted, pure amino compounds were isolated by column chromatography on 100–200 mesh silica gel using ethyl acetate/hexane solvent mixtures as eluents. ^1H and ^{13}C Nuclear magnetic resonance (NMR) spectra were recorded on an Agilent VNMRS PremiumShield spectrometer recording at 600 and 400 MHz. Chemical shifts (δ) were reported in parts per million (ppm) using residual solvent as reference (DMSO- d_6, 2.50 ppm for ^1H and 39.51 ppm for ^{13}C). The NMR splitting patterns are expressed as singlet (s), broad singlet (bs), and multiplet (m).

2.5. Catalytic reduction of 4-nitrophenol by AgNC-1 nanoparticle

In a 25 mL round bottom flux, 4-nitrophenol (1 mmol, 0.1391 g), AgNC-1 (5 mol%, 0.049 g), and H_2O (10 mL) were stirred at room temperature (RT) open to atmosphere. Sodium borohydride (10 mmol, 0.379 g) was added in portion-wise to the stirred suspension over a period of 5 min. The resulting reaction mixture was stirred at 25 °C for 2 h until monitoring by TLC indication complete conversion. The reaction was quenched with saturated NH_4Cl solution (10 mL) and the solution extracted with ethyl acetate (3× 20 mL). The combined organic extract was washed with H_2O (20 mL), brine (20 mL), and dried over anhydrous $MgSO_4$. The solvent was removed under reduced pressure to afford the pure 4-aminophenol as pure white solid (0.1025 g, 94% yield). The product was confirmed by NMR spectroscopy (supporting information).

3. Results and discussion

3.1. Characterization

The surface morphology of silver catalyst AgNC-1 before and after catalytic reaction was investigated by FE-SEM analysis. The microstructural analysis of AgNC-1 confirmed the formation of granular structures of polymer nanocomposite, as seen in Fig. 1a. After 10th cycle of catalytic reaction, some agglomerated granules with rough surface morphology were also evident in the FE-SEM image (Fig. 1b) of the recovered AgNC-1 catalyst. The energy-dispersive X-ray analysis (EDS) spectra (Fig. 1c–d) contained characteristic peaks of carbon, nitrogen, oxygen, sulphur and silver. The presence of 'S' peak in the EDS spectra (Fig. 1c–d) indicated the inclusion of MAA into the PPy matrix. Furthermore, an silver signal in EDS spectra (Fig. 1c–d) also confirmed the presence of Ag NPs on the catalyst surface after adsorption of Ag^+ ions by PPy/MAA composite.

The detailed structure of AgNC-1 catalyst and growth of Ag NPs on the PPy/MAA surface are further revealed by high-resolution TEM images and an electron diffractogram. The HR-TEM image of AgNC-1 catalyst showed (Fig. 2a) an even distribution of nearly spherical Ag NPs on the PPy/MAA surface with an average diameter of 30–40 nm. After 10th cycle of the reaction, Ag NPs distribution

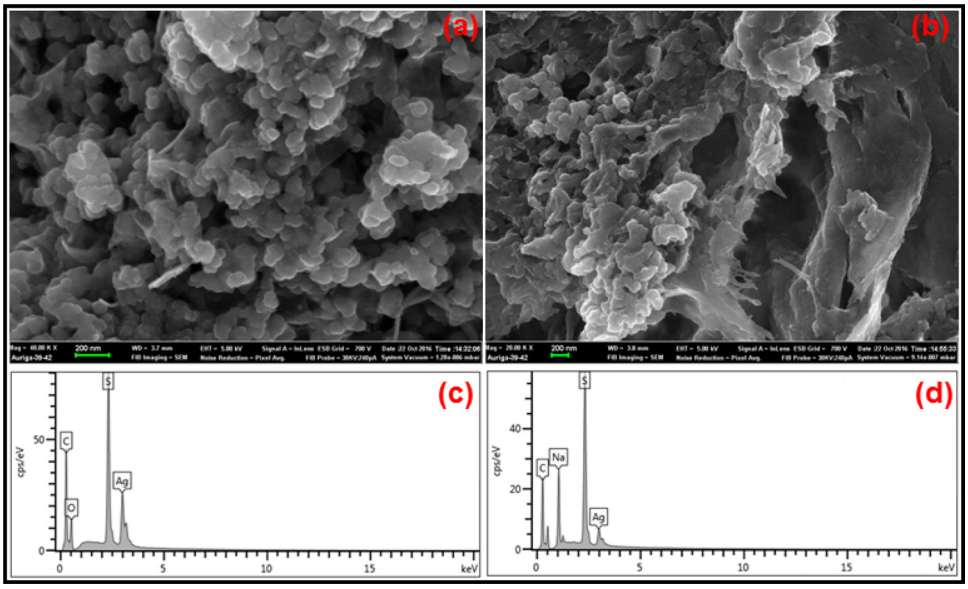

Fig. 1. FE-SEM images of AgNC-1 (a) before catalytic reaction and (b) after the 10th cycle of reaction; EDS spectra of AgNC-1 (c) before and (d) after the 10th reaction cycle.

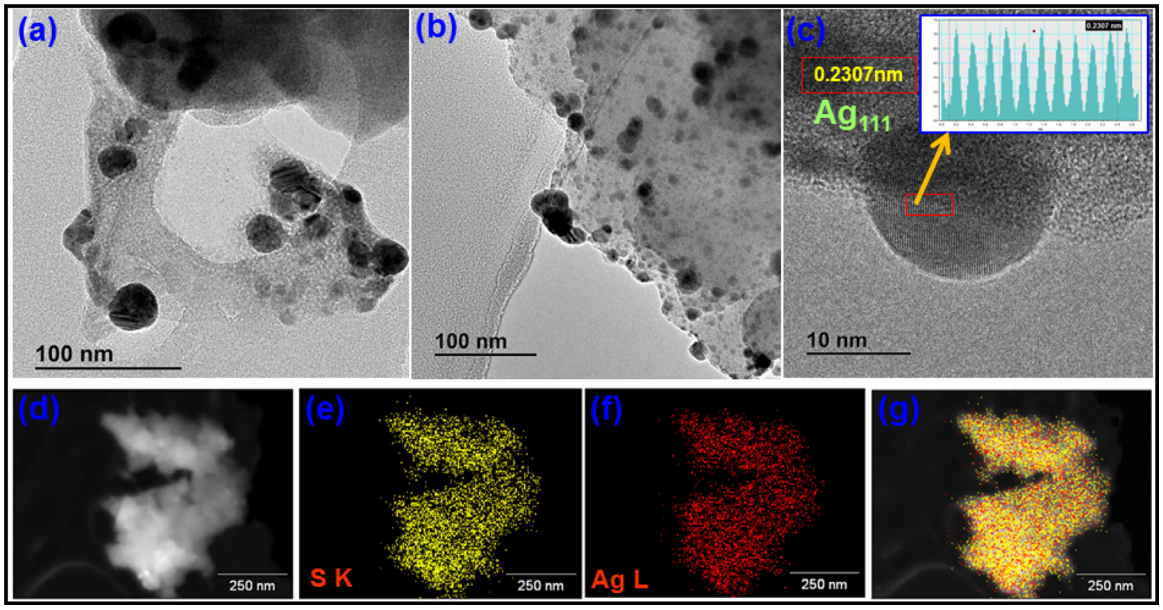

Fig. 2. HR-TEM images of AgNC-1 (a) initial and (b) after the 10th reaction cycle; (c) lattice fringes of the AgNC-1; (d) STEM image of AgNC-1; Homogeneous distribution of (e) 'S' atoms, (f) 'Ag' atoms and (g) combine distribution of 'S' and 'Ag' in the catalyst (AgNC-1) surface.

in AgNC-1 has found as an identical shapes with different particle sizes (Fig. 2b) over the catalyst surface. The interplanar spacing (d-spacing) of crystalline Ag was clearly observed in well-defined lattice fringes of the Ag NPs (Fig. 2c). The observed interplanar distance was found to be $d = 0.2307$ nm (Fig. 2c), related to the (111) diffraction planes of a cubic Ag structure [60,61]. In addition, to better understand the Ag NP growth on PPy/MAA surface, STEM analysis was carried out and the results are shown in Fig. 2(d–g). Fig. 2e and f showed the homogeneous distribution of sulphur and silver on the PPy/MAA surface. Fig. 2g illustrates the even distribution of sulfur (yellow spots) as well as silver (red spots) onto the AgNC-1 catalyst surface.

The FT-IR spectrum of AgNC-1 catalyst is shown (supporting information in Fig. S1) in the range between 4000 and 600 cm^{-1}. The spectrum showed the characteristic bands at 1552 cm^{-1} due to the symmetric and asymmetric ring-stretching modes of PPy ring [62,63], while absorptions at 1358 cm^{-1} and 935 cm^{-1} due to C—N stretching and C—H deformation vibrations of the PPy ring, respectively are also evident. The broad absorption at 3255–3106 cm^{-1} due to stretching vibration of the O—H groups [64] (νOH, COOH), along with the C—H stretching modes of the $-CH_2$ group at 2923 cm^{-1} and the C=O stretching vibration of carboxyl groups at 1695 cm^{-1} confirms the presenceof MAA [65]. A broad adsorption band at the infrared region of 2636–2447 cm^{-1} is attributed to the S—H vibrations [66,67]. The signal at 1261 cm^{-1} is assigned to the C—O stretching frequency of MAA. Therefore, from FT-IR spectrum it can be concluded that thiol functionalized mercaptoacetic acid has been successfully incorporated into polypyrrole composite.

Fig. 3 shows the wide angle powder X-ray diffraction (XRD) patterns of AgNC-1 initially and after 10th catalytic use cycle. The typical XRD patterns of AgNC-1 (Fig. 3a) exhibited five distinguished sharp diffraction peaks at Bragg angles of the 38.12°,

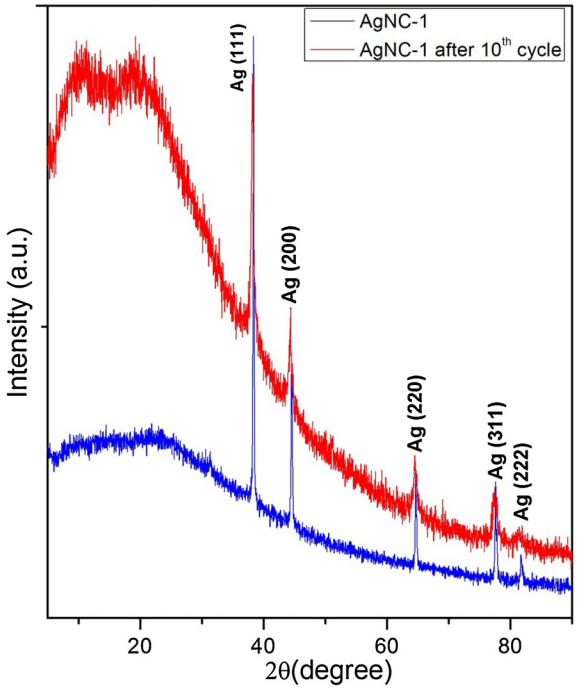

Fig. 3. XRD patterns of AgNC-1 catalyst (a) initial stage and (b) after the 10th reaction cycle.

44.30°, 64.44°, 77.40° and 81.7°, corresponding to the reflections of (111), (200), (220), (311), and (222) crystalline planes of the fcc structure of Ag, respectively [68,69]. These results indicate that the crystalline nature of silver ion was arisen through the reduction of Ag^{+} ions to Ag^{0} by the electron rich polymeric moieties of the adsorbent PPy/MAA [70,71]. It was noted that after 10th use cycles, the fcc structure of AgNC-1 catalyst (Fig. 3b) remained unchanged, as an indication of the catalyst's robustness.

The surface chemical composition and elemental states of AgNC-1 catalyst were investigated by XPS. Fig. 4a presents the XPS survey spectrum of the resulting Ag nanocomposite (AgNC-1), showing that the material contains the elements of C, N, O and Ag. Fig. 4b depicts the high-resolution core level Ag 3d spectrum of the Ag nanoparticles in the catalyst. Two individual peaks at 367.38 eV for Ag $3d^{5/2}$ and at 373.37 eV for Ag $3d^{3/2}$ with 6 eV splitting between the two peaks are evident, confirming that the Ag^{+} ions have been reduced by the PPy/MAA matrix to metallic silver (Ag^{0}) [72–74]. The C 1s spectrum (Fig. 4c) is split into four components: C—C (284.02 eV), C—N (285.61 eV), C—S (286.91 eV), and C—O (288.01 eV). Fig. 5d shows the high resolution XPS spectra for the S 2p peak. The spectra show two spin-orbit components [75,76] : $2p^{3/2}$ and $2p^{1/2}$ near 162.65 and 163.76 eV for sulfur. The XPS spectra of O 1s (Fig. 4e) showed a component at 531.60 eV, which can be assigned to the acid functionality (MAA) present in the AgCN-1 catalyst.

3.2. Catalytic performances of 4-NP at various reaction conditions

The ability of AgNC-1, -2, -3, -4 and -5 waste Ag-based catalysts with different wt% (AgNC-4 and -5, supporting information in Table 1) to reduce nitro groups in aqueous media open to the atmosphere was assessed using a 4- nitrophenol (**1**)/$NaBH_4$ system as benchmark (Table 1). While the reduction of 4-NP has been reported by several research groups [77–81] using silver nanoparticles, in all these cases, a large excess of $NaBH_4$ (74 to ≥1000 times or large excess) was used. In our case, we wanted to limit the use of this material to lessen the impact of the process on the environment in terms of salts produced as by- products. Thus, treatment of **1** with 10-fold excess of $NaBH_4$ and 5 mol% of AgNC-1, -2, -3, -4 or -5 furnished the desired 4- aminophenol (**1a**) in all cases (Table 1, entries 1–3), with AgNC-1 proving to be the most efficient of the three silver catalysts tested, affording the desired product **1a** in 94% yield (Table 1, entry 3). When alcohols were tested as alternatives to water, the yields of **1a** dropped to 51% and 62% with methanol and ethanol, respectively (Table 1, entries 4 and 5). The effect of catalyst loading was then investigated. Reducing the catalyst loading from 5 mol% to 2.5 mol% or 1.5 mol% led to a slight drop in yield (82% and 71%, respectively; Table 1, entries 6 and 7). Using a 5-fold excess of $NaBH_4$ in the presence of either 2.5 mol% or 5 mol% of AgNC-1 afforded **1a** in 67% and 81% yield respectively after prolonged reaction time (Table 1, entries 8 and 9). The reduction proved inefficient with the neat PPy-MAA composite (50 mg), without nanocomposite or additional reductant (Table 1, entries 10–12). These experiments revealed the crucial role of Ag NPs in the catalytic reduction of 4-NP. Additionally, the reduction of 4-NP was tested with molecular hydrogen and formic acid or HCO_2H/Et_3N/ethanol catalytic combination in both reflux and mild reaction conditions, all of which were proved to be inefficient in the presence of AgNC-1 catalyst. Thus, from these optimization studies, the standard reaction conditions for the hydrogenation of nitroarene are: 4-NP (1 equiv.), AgNC-1 catalyst (5 mol%), $NaBH_4$ (10 equiv.) using distilled H_2O as solvent at room temperature (25 °C) for 2 h (Table 1, entry 3). The reaction was also scaled up to a 1 g scale of **1** under standard reaction conditions. The desired product **1a** was obtained in 92% yield with 100% selectivity, with no detectable levels of by-products such as hydroxylamino-, azo- or azoxy-intermediates being present in the sample.

3.3. Catalytic performances of AgNC-1 catalyst for the reduction of various nitroarenes

To further explore the scope and limitations of this reduction method, a variety of substrates having reducible functionality of different types on the nitroarene system were tested under the optimized reaction conditions (Table 2). The present catalytic protocol with AgNC- 1was found to be very efficient and highly selective in reducing various nitroarenes to their corresponding anilines. Electron-rich nitroarenes bearing —OH, —Me, and —OMe substituents (Table 2, entries 1–3), the parent nitrobenzene (Table 2, entry 4), as well as electron-deficient nitroarenes bearing -CO_2Me and —COOH groups (Table 2, entries 5 and 6) proceeded well, selectively affording their corresponding anilines while leaving any remaining functionality intact. The chemoselective reduction of nitroarenes in the presence of reducible groups such as —CO_2Me and —COOH was previously reported by Jiang and co-workers [34]. The reduction of 4-nitrobenzyl alcohol provided the corresponding amine in 78% yield without further reduction of the benzylic alcohol (Table 2, entry 7). Unsurprisingly, the reduction of 4-nitroacetophenone and 4-nitrobenzaldehyde gave an inseparable mixture of the products. The reduction of *m*-dinitrobenzene to *m*-phenylenediamine proceeded in 81% yield (Table 2, entry 8); *m*-nitroaniline similarly furnished *m*-phenylenediamine in 76% yield (Table 2, entry 9). Gratifyingly, no dehalogenation was observed in the reduction of 3-chloronitrobenzene to 3-chloroaniline (Table 2, entry 10). Sterically hindered 2,6-dimethylnitrobenzene underwent smooth reduction in 88% yield (Table 2, entry 11). Conversely, 3-hydroxy-6-methyl-2- nitropyridine proved poorly reactive, furnishing the 2-aminopyridine in modest yield (Table 2, entry 12). Chelation effects associated with two basic nitrogen atoms of the product are assumed to deactivate the catalyst. Although reduction of water soluble 4-NP was faster than other hydrophobic

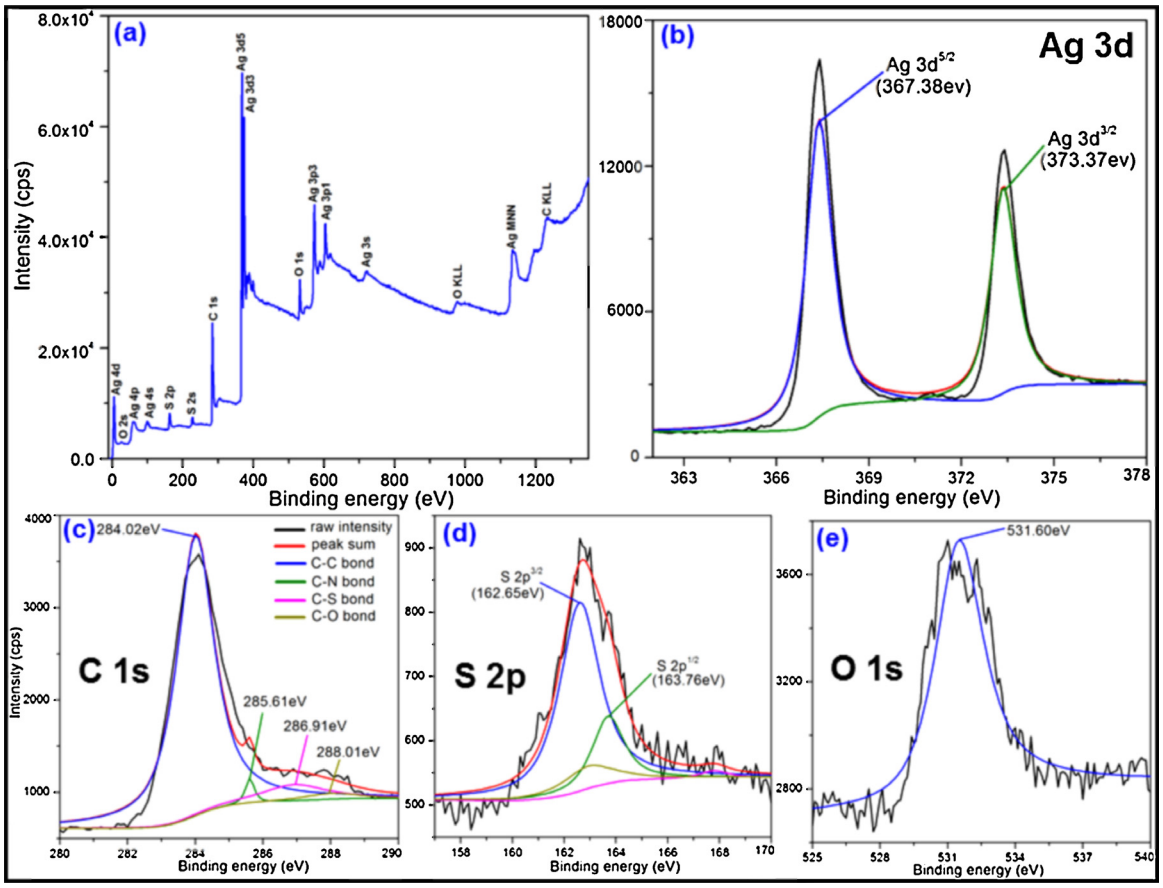

Fig. 4. XPS spectra of AgNC-1 (a) full survey spectrum; (b) high resolution Ag 3d peaks; (c) C 1s peaks; (d) S 2p peaks and (e) O 1s peak.

nitroarenes, the full conversion of such substrates was obtained without any complication.

3.4. Kinetics studies for the reduction of 4-NP using UV-vis spectroscopy

Kinetic investigations of the reduction of 4-NP under the optimized conditions were then performed at 25–55 °C using UV-vis spectrophotometry (Fig. 5). The initially light-yellow 4-NP suspension turned bright yellow upon addition of $NaBH_4$ due to the formation of 4-nitrophenolate ion, which has a corresponding absorbance maximum at λ_{max} = 400 nm [53–55]. After addition of AgNC-1, the bright yellow colour faded slowly over the reaction time, observable as the gradual loss of intensity of the characteristic peak (λ_{max} = 400 nm) and the appearance of two new absorbance maxima at λ_{max} = 300 nm and 230 nm corresponding to the formation of 4-AP [53–55]. Control experiments carried out with PPy-MAA composite and in the absence of AgNC-1 in a similar reaction matrix yielded no change in absorption intensity at 400 nm after stirring for 24 h. These investigations confirmed that AgNC-1 played an important role in the catalytic reduction of 4-NP under our optimized reaction conditions. Moreover, the rate at which the absorbance at 400 nm completely disappeared indicated that the reduction was fairly rapid (Fig. 5). The rate of the reduction was assumed to be independent of the $NaBH_4$ concentration due to addition of excess amount of $NaBH_4$ (~10 times) with respect to 4-NP. Thus, the catalytic reduction could be considered as a pseudo-first-order kinetic model and the rate constants (k) were obtained by Eq. (2) .

$$\ln \frac{C_t}{C_0} = -kt \tag{2}$$

where C_0 is the initial concentration of 4-NP and C_t is the concentration of 4-NP at time 't'. As the absorbance of 4-NP (A) is proportional to the concentration of 4-NP (C), the C_t/C_0 ratio was calculated from a calibration curve (supporting information in Fig S2). The reduction was performed at four different temperatures to obtain rate constants (k) at each temperature. From the linear plot of $\ln(C_t/C_0)$ vs 't', the calculated rate constants (k) at 25 °C, 35 °C, 45 °C, and 55 °C were to be 0.01077 min^{-1}, 0.03338 min^{-1}, 0.07088 min^{-1} and 0.13875 min^{-1}, respectively (R^2 = 0.9901–0.9975; Fig. 6(ii)). In agreement with our observations, the reduction started immediately on addition of AgNC-1. The consumption rates of 4-NP at different temperatures as shown in Fig. 6(i) indicate that the reduction is kinetically facile and does not have an induction period. This contrasts sharply with other known reduction procedures catalyzed by Ag, Pd, and Pt nanocomposites [82,83], all of which have an initial induction time.

Activation energy (E_a) for the catalytic reduction of 4-NP to 4-AP was evaluated from the reaction performed at 25 °C, 35 °C, 45 °C and 55 °C using the Arrhenius Eq. (3).

$$\ln k = \ln A - \frac{E_a}{RT} \tag{3}$$

where k is the rate constant at temperature T (K), A is the Arrhenius factor, and E_a is the apparent activation energy. As represented in Fig. 7, E_a was calculated from the slope of the linear correlation of $\ln k$ vs $10^3/T$, and was estimated to be 68.6 kJ/mol (R^2 = 0.9853).

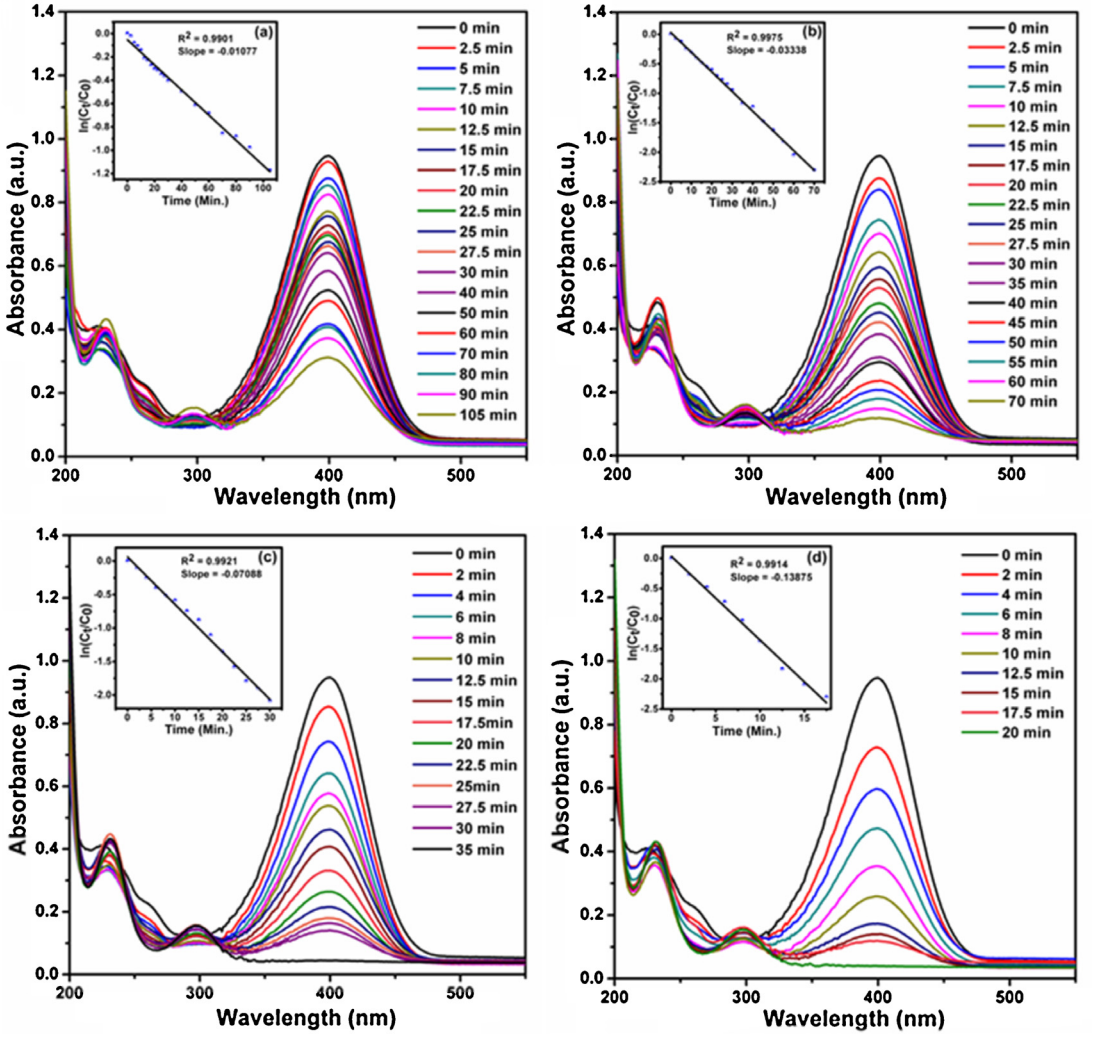

Fig. 5. UV-vis spectra for the catalytic reduction of 4-NP at different temperatures [25 °C (a), 35 °C (b), 45 °C (c), 55 °C (d)].

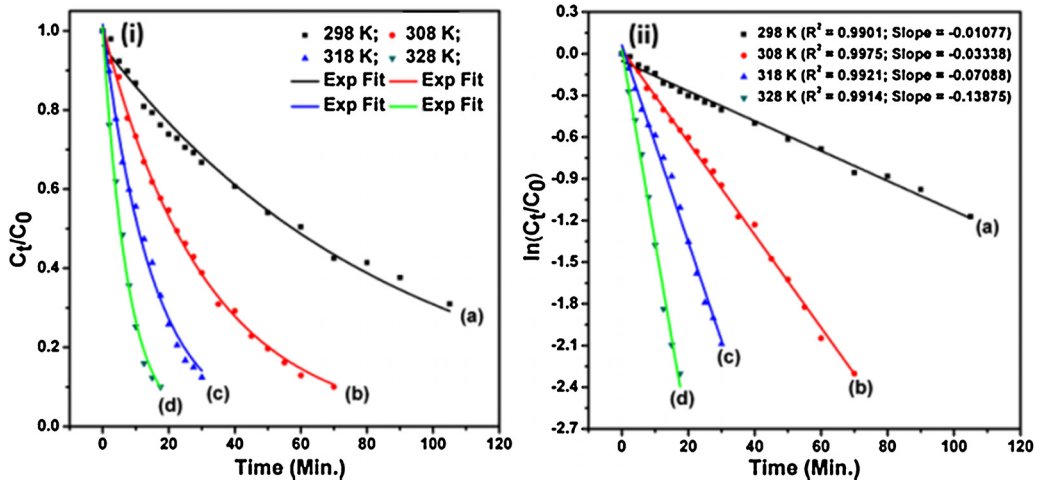

Fig. 6. Plot of ln (C_t/C_0) (i) and (C_t/C_0) (ii) vs time for the reduction of 4-NP at four different temperatures [25 °C (a), 30 °C (b), 35 °C (c), 45 °C (d) and 55 °C (e)].

3.5. *Mechanistic insight for the reduction of 4-nitrophenol*

On the basis of our kinetic studies and related literature [53,54], a mechanism for the catalytic reduction of 4-NP by AgNC-1 is proposed based on the Langmuir–Hinshelwood mechanism (Scheme 1). Initially, borohydride ions (BH_4^-) react with water, forming metaborate (BO_2^-) and hydrogen (H_2). The hydrogen is adsorbed onto the surface of the silver nanoparticles, generating a silver hydride complex as the active reductant. The 4-nitrophenolate anionic substrate and the electron-rich PPy-MAA

Table 2

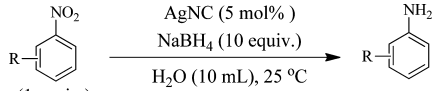

Reduction of nitroarenes using AgNC-1.[a] (1 equiv.)

Entry	Substrate	Product	Time (h)	Yield (%)[b]
1	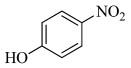	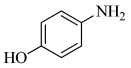 **1a**	2	94
2	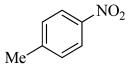	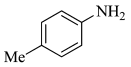 **2a**	5	83
3	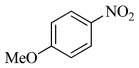	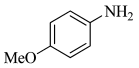 **3a**	4.5	85
4		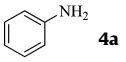 **4a**	3.5	82
5	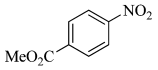	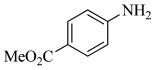 **5a**	6	78
6	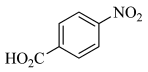	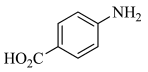 **6a**	5	73
7	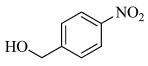	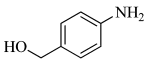 **7a**	1.5	78
8	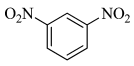	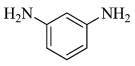 **8a**	0.5	81
9	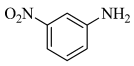	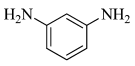	1	76
10	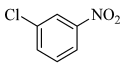	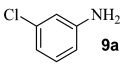 **9a**	4	74
11	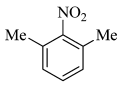	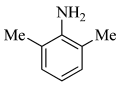 **10a**	2	88
12	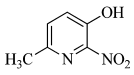	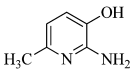 **11a**	6	71

[a] Reaction conditions: nitroarenes (1 mmol), catalyst (5 mol %), water (10 mL), $NaBH_4$ (10 mmol), RT.
[b] Isolated yields.

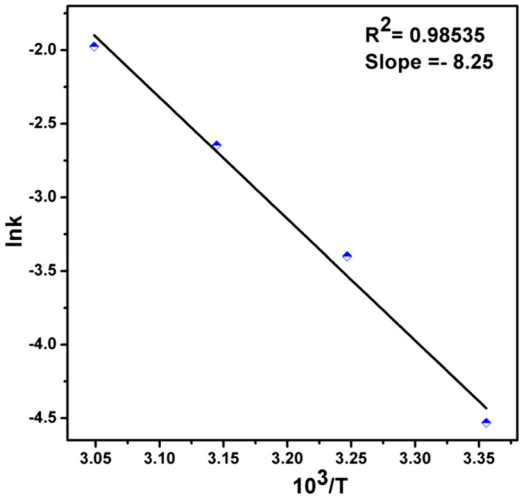

Fig. 7. Arrhenius plot for reduction of **1** with AgNC-1.

matrix then interact through the π–π stacking, putting the substrate in close proximity to the active hydride species bound to the PPy-MAA matrix. Stepwise reduction of the nitro group to the amino product is then accomplished through proposed nitroso and hydroxylamine intermediates with the elimination of water. The intermediary of these species has been confirmed by Ranu and co-workers by LC–MS analysis of the crude reduction mixture of nitrobenzene using Fe NPs [46]. Finally, desorption of 4-AP from the catalyst surface regenerates the starting catalytic species. The lack of a noticeable induction time for this reaction suggests that the rate of adsorption/desorption of reactant and product molecules onto and off of the catalyst surface is very fast [84], implying that one or more of the hydride transfer steps is rate-limiting.

3.6. Catalyst recycling performances

In general, the reusability of metal catalyst is highly desirable from both the industrial, as well as the ecological point of view. Therefore, to diminish the cost- effectiveness of the present catalytic system, the reusability test for the reduction of 4-NP was performed with $NaBH_4$ in the presence of AgNC-1 nanocatalyst under standard reaction conditions. After each experiment, AgNC-1 catalyst was filtered from the reaction mixture using 0.45 μm cellulose filter paper. The recovered catalyst was washed three

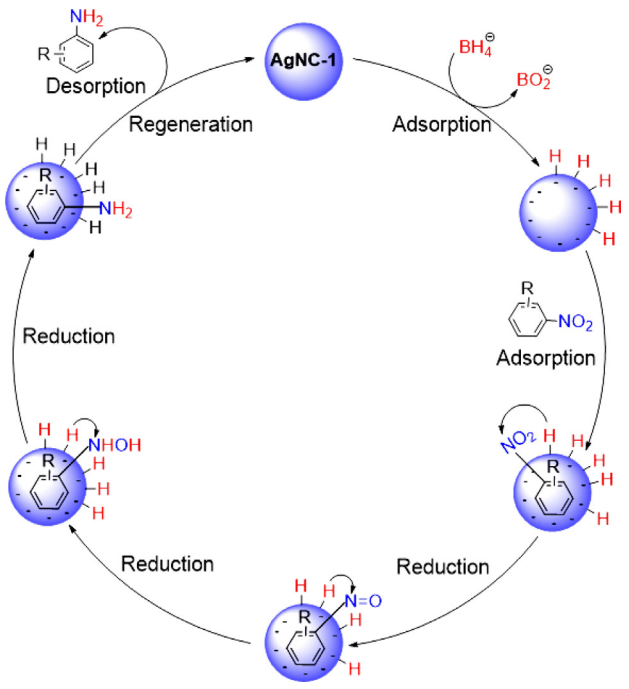

Scheme 1. Proposed mechanism for the catalytic reduction of 4-NP by AgNC-1 based on Langmuir–Hinshelwood mechanism.

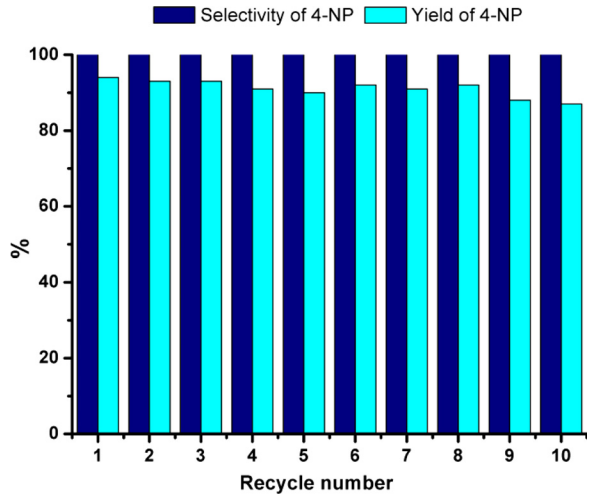

Fig. 8. Reusability of AgNC-1 for reduction of 4-NP.

times with 25 mL deionized water and 20 mL acetone to remove the organic residue. Then, the catalyst was dried under high vacuum for 1 h and reused for next cycle. In a similar way, AgNC-1 catalyst was tested for consecutive 10 cycles under similar reaction conditions. Noteworthy is that no significant loss of the catalytic activity and selectivity was observed after 10 cycles, as shown in Fig. 8. Well distribution (Fig. 2b) and fine crystallinity (Fig. 3b) of Ag NPs remains unaffected even though after 10 cycles. The desired product, 4- aminophenol, was obtained in average 92% yield with 100% selectivity. To test the stability and heterogeneity of the AgNC-1 nanoparticles, ICP-MS measurement was performed. No significant Ag leaching (~0.1 ppm in 1st cycle and ~0.15 ppm Ag in 10th cycle) into the supernatant after 1st and 10th cycle was observed by ICP-MS, confirming that the AgNC-1 catalyst is extremely stable under these conditions over 10 cycles.

4. Conclusion

In conclusion, the economical, mild, and cost-effective catalytic hydrogenation of various nitroarenes under different using PPy-MAA supported Ag-adsorbed waste nanoparticles at room temperature in water was explored. A wide variety of substituents are well- tolerated on the aryl ring, including —CO_2Me, —CO_2H, and —Cl, with high selectivity and specificity for the reduction of the nitro group in good yields having been demonstrated. Kinetic studies have demonstrated that the reduction is facile, involves no induction period, and that the catalyst is readily amenable to recycling at least ten times without significant loss of its selectivity, reactivity or leaching of the metal from the support. Thus, a PPy-MAA silver nanocomposite, essentially a waste product from the remediation of waste water, has been demonstrated to be a practical source of AgNPs for chemical catalysis under standard reaction protocols. The material is a non-hazardous, sustainable heterogeneous catalyst, useful in the elimination of the intractable pollutant 4-nitrophenol from aqueous media, and is very active in the catalytic reduction of functionalized aromatic nitro derivatives, important industrial intermediates for the synthesis of analgesic and antipyretic drugs.

Acknowledgements

S.G. thanks the University of South Africa for Post-Doctoral Fellowship Award-2015. AM thanks to Water Research Commission (WRC), National Research Foundation (NRF) and Council for Scientific and Industrial Research (CSIR), South Africa for their financial support. A.M. also thanks to DST/CSIR National Centre for Nano Structured Material and Dr. Gerda Fouche of CSIR-Bioscience Pretoria, South Africa for providing the infrastructure. Nanostructured Materials characterization unit is also acknowledged for materials characterization.

Appendix A. Supplementary data

Supplementary data associated with this article can be found, in the online version, at http://dx.doi.org/10.1016/j.apcatb.2017.03.033.

References

[1] M. Benaglia, Recoverable and Recyclable Catalysts, John Wiley & Sons, Chichester, 2009.
[2] E.S. Beach, Z. Cui, P.T. Anastas, Energy Environ. Sci. 2 (2009) 1038–1049.
[3] A.F. Lee, J.A. Bennett, J.C. Manayil, K. Wilson, Chem. Soc. Rev. 43 (2014) 7887–7916.
[4] R.A. Sheldon, Chem. Soc. Rev. 41 (2012) 1437–1451.
[5] S.L.Y. Tang, R.L. Smith, M. Poliakoff, Green Chem. 7 (2005) 761–762.
[6] G. Centi, S. Perathoner, Catal. Today 77 (2003) 287–297.
[7] D. Prat, A. Wells, J. Hayler, H. Sneddon, C.R. McElroy, S. Abou-Shehada, P.J. Dunn, Green Chem. 18 (2016) 288–296.
[8] Q.-F. Shi, G.W. Diao, Electrochim. Acta. 58 (2011) 399–405.
[9] Y.-X. Sua, B.-X. Fan, L.-S. Wang, Y.-F. Liu, B.-C. Huang, M.-L. Fu, L.-M. Chen, D.-Q. Ye, Catal. Today 201 (2013) 115–121.
[10] C. Yuan, Y. Xu, W. Luo, B. Zeng, W. Qiu, J. Liu, H. Huang, L. Dai, Nanotechnology 23 (2012) 175301–175309.
[11] F. Cardenas-Lizana, S. Gomez-Quero, N. Perret, M.A. Keane, Catal. Sci. Technol. 1 (2011) 652–661.
[12] J. Horacek, G. Stavova, V. Kelbichova, D. Kubicka, Catal. Today 204 (2013) 38–45.
[13] A. Yoshida, Y. Mori, T. Ikeda, K. Azemoto, S. Naito, Catal. Today 203 (2013) 153–157.
[14] V. Polshettiwar, R.S. Varma, Green Chem. 12 (2010) 743–754.
[15] R.S. Varma, ACS Sustain. Chem. Eng. 4 (2016) 5866–5878.
[16] D. Astruc, F. Lu, J.R. Aranzaes, Angew. Chem. Int. Ed. 44 (2005) 7852–7872.
[17] H. Rong, S. Cai, Z. Niu, Y. Li, ACS Catal. 3 (2013) 1560–1563.
[18] L. Li, Z. Niu, S. Cai, Y. Zhi, H. Li, H. Rong, L. Liu, L. Liu, W. He, Y. Li, Chem. Commun. 49 (2013) 6843–6845.
[19] S. Cai, D. Wang, Z. Niu, Y. Li, Chin. J. Catal. 34 (2013) 194–1974.

[20] H. Rong, Z. Niu, Y. Zhao, H. Cheng, Z. Li, L. Ma, J. Li, S. Wei, Y. Li, Chem. Eur. J. 21 (2015) 12034–12041.
[21] S.C. Mitchell, R.H. Waring, Ullmanns Encyclopedia of Industrial Chemistry, Wiley-VCH Verlag, Weinheim, Germany, 2000.
[22] N. Ono, The Nitro Group in Organic Synthesis, Wiley-VCH, New York, 2001.
[23] S.A. Lawrence, Amines: Synthesis, Properties and Applications, Cambridge University Press, New York, 2004.
[24] S. Cai, H. Duan, H. Rong, D. Wang, L. Li, W. He, Y. Li, ACS Catal. 3 (2013) 608–612.
[25] L. Luo, K. Xu, R. Zang, L. Juang, J. Wang, W. Xing, J. Huang, Catal. Sci. Technol. 2 (2012) 301–304.
[26] W.-G. Jia, H. Zhang, T. Zhang, D. Xie, S. Ling, E.-H. Sheng, Organometallics 35 (2016) 503–512.
[27] M. Takasaki, Y. Motoyama, K. Higashi, S.-H. Yoon, I. Mochida, H. Nagashima, Org. Lett. 10 (2008) 1601–1604.
[28] P. Lara, K. Philippot, Catal. Sci. Technol. 4 (2014) 2445–2465.
[29] K. Tsutsumi, F. Uchikawa, K. Sakai, K. Tabata, ACS Catal. 6 (2016) 4394–4398.
[30] J. Sun, Y. Fu, G. He, X. Sun, S. Wang, Catal. Sci. Technol. 4 (2014) 1742–1748.
[31] S. Fountoulaki, V. Daikopoulou, P.L. Gkizis, I. Tmiolakis, G.S. Armatas, I.N. Lykakis, ACS Catal. 4 (2014) 3504–3511, and the references cited therein.
[32] K. Shimizu, Y. Miyamoto, A. Satsuma, J. Catal. 270 (2010) 86–94.
[33] C.-Y. Wang, C.-F. Fu, Y.-H. Liu, S.-M. Peng, S.-T. Liu, Inorg. Chem. 46 (2007) 5779–5786.
[34] C. Jiang, Z. Shang, X. Liang, ACS Catal. 5 (2015) 4814–4818.
[35] R.D. Patil, Y. Sassona, Org. Chem. Curr. Res. 4 (2015) 154.
[36] C. Boix, M. Poliakoff, J. Chem. Soc. Perkin Trans. 1 (1999) 1487–1490.
[37] A. Saha, B.C. Ranu, J. Org. Chem. 73 (2008) 6867–6870.
[38] H.D. Burge, D.J. Collins, B.H. Davis, Ind. Eng. Chem. Prod. Res. Dev. 19 (1980) 389–391.
[39] R.M. Deshpande, A.N. Mahajan, M.M. Diwakar, P.S. Ozarde, R.V. Chaudhari, J. Org. Chem. 69 (2004) 4835–4838.
[40] L. Pehlivan, E. Metay, S. Laval, W. Dayoub, P. Demonchaux, G. Mignani, M. Lemaire, Tetrahedron Lett. 51 (2010) 1939–1941.
[41] L. Liu, B. Qiao, Z. Chen, J. Zang, Y. Deng, Chem. Commun. 51 (2009) 653–655.
[42] A. Corma, P. Serna, Science 313 (2006) 332–334.
[43] K. Layek, M.L. Kantam, M. Shirai, D. Nishio-Hamane, T. Sasaki, H. Maheswaren, Green Chem. 14 (2012) 3164–3174.
[44] R.V. Jagadeesh, K. Natte, H. Junge, M. Beller, ACS Catal. 5 (2015) 1526–1529.
[45] R.V. Jagadeesh, A.-E. Surkus, H. Junge, M.-M. Pohl, J. Radnik, J. Rabeah, H. Huan, V. Schunemann, A. Bruckner, M. Beller, Science 342 (2013) 1073–1076.
[46] R. Dey, N. Mukherjee, S. Ahammed, B.C. Ranu, Chem. Commun. 48 (2012) 7982–7984.
[47] N.M. Patil, T. Sasaki, B.M. Bhanage, ACS Sustain. Chem. Eng. 4 (2016) 429–436.
[48] S. Sharma, M. Kumar, V. Kumar, N. Kumar, J. Org. Chem. 79 (2014) 9433–9439.
[49] T. Vincent, E. Guibal, Langmuir 19 (2003) 8475–8483.
[50] A.S. Travis, Manufacture and Uses of the Anilines: A Vast Array of Processes and Products, The Chemistry of Anilines Part 1, Wiley, 2009, pp. 764.
[51] O.A. O'Connor, L.Y. Young, Environ. Toxicol. Chem. 8 (1989) 853–862.
[52] M.A. Oturan, J. Peiroten, P. Chartrin, A.J. Acher, Environ. Sci. Technol. 34 (2000) 3474–3479.
[53] J. Xia, G. He, L. Zhang, X. Sun, X. Wang, Appl. Catal. B 180 (2016) 408–415.
[54] P. Zhao, X. Feng, D. Huang, G. Yang, D. Astruc, Coord. Chem. Rev. 287 (2015) 114–136.
[55] X. Li, K. Wu, Y. Ye, X. Wei, Nanoscale 5 (2013) 3648–3653.
[56] N. Pradhan, A. Pal, T. Pal, Colloids Surf. A 196 (2002) 247–257.
[57] S. Giri, M. Bhaumik, R. Das, V.K. Gupta, A. Maity, Appl. Catal. B 202 (2017) 207–216.
[58] S. Machida, S. Miyata, Synth. Met. 31 (1989) 311–318.
[59] C. Li, C. Liu, F. Li, Q. Gong, Chem. Phys. Lett. 380 (2003) 201–205, and reference cited therein.
[60] X. Ding, G. Briggs, W. Zhou, Q. Chen, L.M. Peng, Nanotechnology 17 (2006) S376–S380.
[61] X. Yan, S. Li, J. Bao, N. Zhang, B. Fan, R. Li, X. Liu, Y.X. Pan, ACS Appl. Mater. Interfaces 8 (2016) 17060–17067.
[62] X. Zhang, J. Zhang, W. Song, Z. Liu, J. Phys. Chem. B 110 (2006) 1158–1165.
[63] G. Cho, B.M. Fung, D.T. Glatzhofer, J.S. Lee, Y.G. Shul, Langmuir 17 (2001) 456–461.
[64] M. Koneswaran, R. Narayanaswamy, Sens. Actuators B 139 (2009) 91–96.
[65] A.E. Vikraman, A.R. Jose, M. Jacob, K.G. Kumar, Anal. Methods 7 (2015) 6791–6798.
[66] F. He, W. Wang, J.W. Moon, J. Howe, E.M. Pierce, L. Liang, ACS Appl. Mater. Interfaces 4 (2012) 4373–4379.
[67] S.T. Song, N. Saman, K. Johari, H. Mat, Chem. Res. 52 (2013) 13092–13101.
[68] S. Bhattarai, J.S. Kim, Y.S. Yun, Y.S. Lee, React. Funct. Polym. 105 (2016) 52–59.
[69] Y. Yao, B. Gao, F. Wu, C. Zhang, L. Yang, ACS Appl. Mater. Interfaces 7 (2015) 10634–10640.
[70] Q.F. Lü, J.J. Luo, T.T. Lin, Y.Z. Zhang, ACS Sustain. Chem. Eng. 2 (2014) 465–471.
[71] J. Huang, Z. Yang, RSC Adv. 5 (2015) 33814–33817.
[72] Q. Deng, X. Duan, H.L. Dickon, H. Tang, Y. Yang, M. Kong, ACS Appl. Mater. Interfaces 4 (2012) 6030–6037.
[73] C. Chen, Y. Zheng, Y. Zhan, X. Lin, Q. Zheng, K. Wei, Dalton Trans. 40 (2011) 9566–9570.
[74] S.A. Ansari, M.M. Khan, M.O. Ansari, J. Lee, M.H. Cho, J. Phys. Chem. C. 117 (2013) 27023–27030.
[75] R. Vitaliano, I. Fratoddi, I. Venditti, G. Roviello, C. Battocchio, G. Polzonetti, M.V. Russo, J. Phys. Chem. A. 113 (2009) 14730–14740.
[76] G. Gonella, O. Cavalleri, S. Terreni, D. Cvetko, F. Floreano, A. Morgante, M. Canepa, R. Rolandi, Surf. Sci. 566–568 (2004) 638–643.
[77] T. Wu, L. Zhang, J. Gao, Y. Liu, C. Gao, J. Yan, J. Mater. Chem. A 1 (2013) 7384–7390.
[78] P. Zhang, Y. Sui, G. Xiao, Y. Wang, C. Wang, B. Liu, G. Zou, B. Zou, J. Mater. Chem. A 1 (2013) 1632–1638.
[79] S. Tang, S. Vongehr, X. Meng, J. Phys. Chem. C 114 (2010) 977–982.
[80] Z. Wang, S. Zhai, B. Zhai, Z. Xiao, F. Zhang, Q. An, New J. Chem. 38 (2014) 3999–4006.
[81] T. Ji, L. Chen, M. Schmitz, F.S. Bao, J. Zhu, Green Chem. 17 (2015) 2515–2523.
[82] Y. Mei, Y. Lu, F. Polzer, M. Ballauff, M. Drechsler, Chem. Mater. 19 (2007) 1062–1069.
[83] Y. Lu, Y. Mei, M. Drechsler, M. Ballauff, Angew. Chem. Int. Ed. 45 (2006) 813–816.
[84] W. Shen, Y. Qu, X. Pie, S. Li, S. You, J. Wang, Z. Zang, J. Zhou, J. Hazard. Mater. 321 (2017) 299–306.